

A Suzaku Observation of the Low-Ionization Fe-Line Emission from RCW 86

Masaru UENO,¹ Rie SATO,¹ Jun KATAOKA,¹ Aya BAMBA,² Ilana HARRUS,^{3,4}
Junko HIRAGA,² John P. HUGHES,⁵ Caroline A. KILBOURNE,⁴ Katsuji KOYAMA,⁶
Motohide KOKUBUN,⁷ Hiroshi NAKAJIMA,⁶ Masanobu OZAKI,⁸ Robert PETRE,⁴
Tadayuki TAKAHASHI,⁸ Takaaki TANAKA,⁸ Hiroshi TOMIDA,⁹ and Hiroya YAMAGUCHI⁶

¹*Department of Physics, Faculty of Science, Tokyo Institute of Technology,
2-12-1, Meguro-ku, Ohokayama, Tokyo 152-8551, Japan*

E-mail(MU): masaru@hp.phys.titech.ac.jp

²*RIKEN (The Institute for Physics and Chemical Research)*

2-1, Hirosawa, Wako-shi, Saitama, Japan

³*Department of Physics and Astronomy, Johns Hopkins University, Baltimore, MD, 21218, USA*

⁴*NASA Goddard Space Flight Center, X-ray Astrophysics Laboratory, Code 662,
Greenbelt, MD 20771, USA*

⁵*Department of Physics and Astronomy, Rutgers University
136 Frelinghuysen Road, Piscataway, NJ 08854-8109, USA*

⁶*Department of Physics, Graduate School of Science, Kyoto University,
Sakyo-ku, Kyoto 606-8502, Japan*

⁷*Department of Physics, University of Tokyo, 7-3-1 Hongo, Bunkyo-ku, Tokyo, Japan*

⁸*Institute of Space and Astronautical Science, Japan Aerospace Exploration Agency
3-1-1 Yoshinodai, Sagami-hara, Kanagawa 229-8510, Japan*

⁹*ISS Science Project Team, Institute of Space and Astronautical Science,
Japan Aerospace Exploration Agency 2-1-1, Sengen, Tsukuba, Ibaraki 305-8505, Japan*

(Received ; accepted)

Abstract

The newly operational X-ray satellite Suzaku observed the southwestern quadrant of the supernova remnant (SNR) RCW 86 in February 2006 to study the nature of the 6.4 keV emission line first detected with the Advanced Satellite for Cosmology and Astronomy (ASCA). The new data confirm the existence of the line, localizing it for the first time; most of the line emission is adjacent and interior to the forward shock and not at the locus of the continuum hard emission. We also report the first detection of a 7.1 keV line that we interpret as the $K\beta$ emission from low-ionization iron. The Fe-K line features are consistent with a non-equilibrium plasma of Fe-rich ejecta with $n_e t \lesssim 10^9 \text{ cm}^{-3} \text{ s}$ and $kT_e \sim 5 \text{ keV}$. This combination of low $n_e t$ and high kT_e suggests collisionless electron heating in an SNR shock. The Fe $K\alpha$ line shows evidence for intrinsic broadening, with a width of 47 (34–59) eV (99% error region). The difference of the spatial distributions of the hard continuum above 3 keV and the Fe-K line emission support a synchrotron origin for the hard continuum.

Key words: shock waves – ISM: supernova remnants – ISM: individual (RCW 86) – X-rays: ISM

1. Introduction

Since the first discovery, in SN 1006, of synchrotron X-ray emission from a supernova remnant shell (Koyama et al. 1995), similar X-ray emission characteristics have been found in a number of young SNRs [see for example, Cas A (Hughes et al. 2000); Tycho (Hwang et al. 2002); or G347.3–0.5 (Slane et al. 2001)]. This X-ray synchrotron emission is usually interpreted as coming from electrons with energy up to 10 TeV and is the strongest evidence to date of particle acceleration in the diffuse shocks of young SNRs.

RCW 86 is one of the SNRs in which such X-ray synchrotron emission has been discovered. It has in addition some high-energy emission associated with a low-

ionization Fe-K line and localized in the southwest part of the remnant. This line was discovered in 1997 in the ASCA observations of the remnant (Vink et al. 1997) and confirmed subsequently using BeppoSAX (Bocchino et al. 2000). The origin of both the line and the high-energy X-ray emission remain a mystery. In their initial paper, Vink et al. (1997) conjectured that the strong 6.4 keV line and the hard X-ray emission could be explained by an electron distribution with a supra-thermal tail. The BeppoSAX observations revealed spatial variations in the hardness ratio of the emission and favored a two-temperature plasma model, mixing a low-abundance, low-temperature component with a high-abundance, high-temperature counterpart. The high-temperature component was interpreted as Fe-rich ejecta and the low tem-

perature component as circumstellar medium (Bocchino et al. 2000). The detection of high-energy (> 10 keV) emission by RXTE (Petre et al. 1999) suggests the existence of non-thermal X-ray emission. Bamba et al. (2000) and Borkowski et al. (2001a) found that the ASCA spectrum from the SW region can be explained by a combination of three components: low and high temperature plasmas, and non-thermal (synchrotron) emission. Using the superior high spatial resolution of Chandra, Rho et al. (2002) spatially resolved the low-temperature plasma and the hard continuum emission. By showing a spatial correlation between the hard continuum and radio emission, they provided strong evidence that the hard continuum originates from synchrotron emission. Since they found the Fe $K\alpha$ line arises only from the region of the hard continuum, they suggested that the synchrotron X-rays are emitted from Fe-rich ejecta. Hard X-ray emission from the northeast rim of RCW 86 shows no evidence for a 6.4 keV line, and Vink et al. (2006) has suggested this emission is synchrotron.

Since the spatial distribution of the 6.4 keV-line and precise spectroscopy of the line features provide important information about the emission mechanism of the line, we performed a Suzaku observation of the southwestern quadrant of RCW 86. In this paper, we mainly report on the results in the hard band (> 3 keV): the hard continuum and Fe line features. We assume a kinematic distance of 3 kpc (Rosado et al. 1996).

2. SUZAKU Observation of RCW 86

Suzaku is a joint Japanese-US mission that was launched in July 2005 (Mitsuda et al. 2006). Two instruments, the XIS and HXD, are operational. The XIS consists of 4 independent CCDs cameras, three front-illuminated (energy range 0.4–12 keV) and one back-illuminated (energy range 0.2–12 keV). Each is located in the focal plane of a dedicated nested thin-foil X-ray telescope (XRTs). The total effective area is quite large (~ 1000 cm $^{-2}$ at 6 keV). In addition, the low-Earth orbit of Suzaku provides a low, reproducible background environment. The HXD is a non-imaging collimated detector which extends the bandpass of the observatory up to 600 keV. More information on the mission and the instruments on board (XRT, XIS, and HXD) can be found in Serlemitsos et al. (2006), Koyama et al. (2006), and Takahashi et al. (2006).

The southwest quadrant of RCW 86 was observed by Suzaku in February 2006. At the writing of this paper, the background determination for the HXD is still not complete and we chose not to include any HXD data in our analysis. The XIS contamination (Koyama et al. 2006) plays no role at the energies of the Fe-K line, our main concern for this paper.

The data (revision 0.7; Mitsuda et al. 2006) were analyzed after the following filtering. Data taken with low data rate, at low elevation angle from the Earth rim ($< 5^\circ$), or during passage through the South Atlantic Anomaly were removed. We also removed data from hot and flick-

ering pixels using the `cleansis` software. In order to suppress the hard-band background of XIS 1, which is higher than that of XIS 0, 2, or 3, data taken at low cut-off rigidity regions (< 6 GV) were also removed from the XIS 1 data. The resultant exposure times are 116 ks for each XIS 0, 2, 3 and 96 ks for XIS 1. At this stage of the mission, the attitude is not completely correct and we used a point source detected in an XMM-Newton observation of RCW 86, to correct the absolute coordinate system of our observation. The correction is rather small ($\Delta RA = -0^\circ 0044$, $\Delta Dec = -0^\circ 0049$) for all 4 of the XIS.

3. XIS Images

Figures 1a and b show XIS intensity contours in the low (0.5–1.0 keV) and high (3.0–6.0 keV) energy bands. The high-energy band was chosen to show the contribution from the continuum only. Overlaid on the low energy contours in Fig. 1a is the 6.4 keV line intensity image. This image was generated by subtracting an estimated continuum level from the (6.34–6.46 keV) image. The continuum contribution was estimated by scaling the (5.0–6.2 keV) image using a power-law model. Since smoothing may introduce artificial structures, we adaptively binned the image using the weighted Voronoi tessellation algorithm implemented by Diehl & Statler (2006), which is based on the algorithm of Cappellari & Copin (2003). The size of each bin was determined so that significance of the 6.4 keV line is at least 5σ . The resulting image is shown superposed on the high energy contours in Fig. 1b. In order to quantify the spatial correlation between the 6.4 keV line and the continuum emission, we furthermore obtained the spatial variation of count-rate ratios between the 6.4 keV line and the (5.0–6.2 keV) band using the same binning. The result is shown in Fig. 2 with the 3.0–6.0 keV intensity contours. If we multiply this ratio by 3, it corresponds to the equivalent width (keV) of the 6.4 keV line at that position. We have generated in Fig. 3 a true color image of the remnant showing the spatial variations between low and high-energy continuum (shown in blue and red respectively), and the 6.4 keV-line (shown in green).

The spatial distribution of the 6.4 keV line is revealed for the first time, thanks to the combination of Suzaku's large effective area and low background around 6.4 keV. The red region in Fig. 3, corresponding to the location of the low-temperature plasma, was attributed to the forward shock by Rho et al. (2002). The blue region corresponds to hard, filamentary structures revealed by the Chandra observation (Rho et al. 2002). The 6.4 keV line is emitted primarily from the interior to the forward shock region. As apparent in Fig 1b, the high-energy continuum emission does not correlate with the intensity peak of the 6.4 keV line. Fig. 2 shows instead that the equivalent width of the 6.4 keV line and the continuum emission anti-correlate with each other, and thus probably have different origins. In Fig. 4, we demonstrate that there is good spatial correlation between the 6.4 keV line and the radio continuum emission (MOST 843MHz; Whiteoak & Green 1996). Since radio continuum emission is often found in

Table 1. Suzaku Observations Appearing in this Paper.

Target	Observation ID	Date	Exposure ^a (ks)
RCW 86 Southwest	500004010	2006/02/12–14	116.5/96.4
North Ecliptic Polar	500026010	2006/02/10–12	96.0/87.5
High Latitude A	500027010	2006/02/14–15	79.5/71.1
Sgr C	500018010	2006/02/20–23	114.5/98.6

^aExposure times for XIS0,2,3/XIS1 after the data screening.

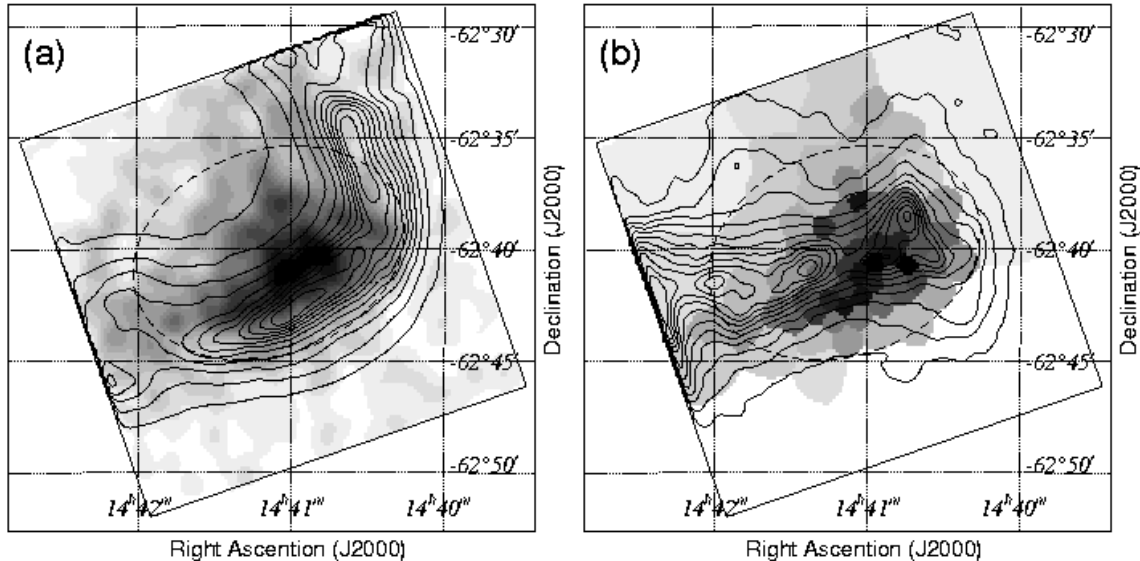


Fig. 1. XIS 0.5–1.0 keV (a) and 3.0–6.0 keV (b) intensity contours overlaid by the 6.4 keV-line images. The 6.4 keV line image in (a) is smoothed with a Gaussian kernel of $\sigma=25''$, whereas that in (b) is adaptively binned using the weighted Voronoi tessellation algorithm (Diehl & Statler 2006). Images and contours are plotted using a linear scale. The spectral region is shown with a broken-line ellipse. The XIS field of view is designated with a solid-line square in each image.

the downstream of a shock, which is also pointed out for the southwest region of RCW 86 (Rho et al. 2002), the 6.4 keV line is likely to be emitted from the downstream of a shock. We will examine below how the spectral analysis of the line fit with this new finding.

4. Spectral Analysis of the 6.4 keV Line

In order to study the origin of the 6.4 keV emission line, we extracted spectra from an elliptical region centered at $(14^{\text{h}}41^{\text{m}}08^{\text{s}}.7, -62^{\circ}40'10'')$, with 12.5×9.2 major and minor axes and a position angle of 20° . This region is demarcated by the dashed line in Fig. 1. It was chosen to provide the maximum signal-to-noise ratio for the 6.4 keV line. While one might expect distinct spectra from the red, green and blue regions in Fig. 2, the spatial resolution of XIS does not allow such distinct separation. Moreover, Chandra and XMM-Newton are better suited for spatially resolved spectroscopy of the soft component and the hard continuum emission. Therefore we concentrate here on the spectroscopy of the Fe-K line region.

As the entire XIS field of view is covered by the remnant, we used “blank-sky” observations for background spectra, extracting the background from the same regions

on the detectors as the ones used in the analysis. The two observations used to provide background spectra (“North Ecliptic Polar” and “High Latitude A”, see Table 1) were carried out immediately before and after the RCW 86 observation, insuring an identical detector response. Spectra from these two observations were weighted averaged using their exposure times. Above 3 keV, differences between the responses from all the FI chips are negligible; we therefore summed the spectra from XIS 0, 2 and 3 for the following analysis. Although the BI spectrum is analyzed separately, the differences between the best fit parameters from the two spectra are negligible.

Background-subtracted 3.0–10 keV spectra are shown in Fig. 5. Since the spectrum appears flat with the exception of two conspicuous lines at 6.4 and 7.1 keV, we fitted it using a power-law model plus two Gaussians corrected for the interstellar absorption. Since the absorption column is not well determined by these hard band spectra, we fixed the column density N_{H} at $5 \times 10^{21} \text{ cm}^{-2}$, which is close to the values obtained by Rho et al. (2002) for the SW regions. The fit results have no strong dependence on the column density. The standard RMF files version 2006-02-13 were used, whereas ARF files were produced by the `xissimarfgen` software version 2006-05-28 with CALDB

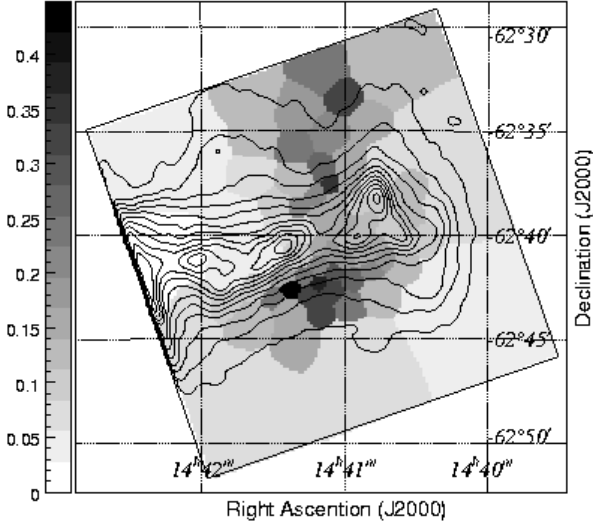


Fig. 2. Count-rate ratio map between the 6.4 keV line and the 5.0–6.2 keV band overlaid with contours of the 3.0–6.0 keV intensity map. An equivalent width (in keV) of the 6.4 keV line can be obtained by multiplying this ratio by a factor of 3.

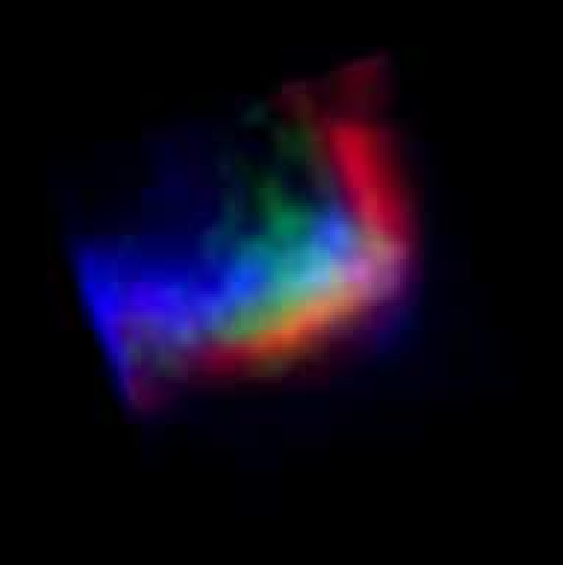


Fig. 3. True color XIS image of the RCW 86 southwestern region: red represents 0.5–1.0 keV photons; blue represents 3.0–6.0 keV photons; and green represents 6.4 keV emission.

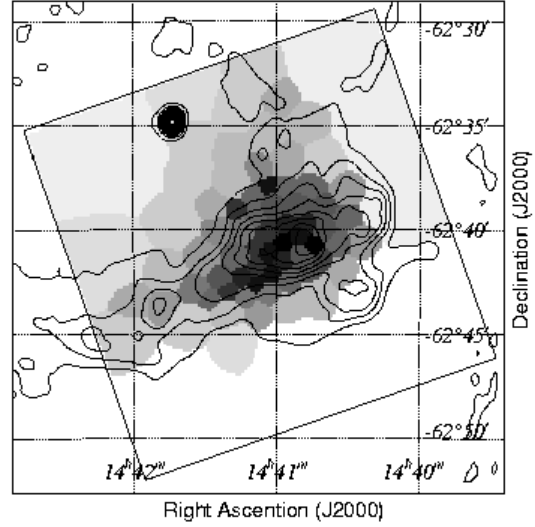


Fig. 4. Intensity contours of the MOST 843 MHz radio continuum (Whiteoak & Green 1996) overlaid by the 6.4 keV-line image. Images and contours are plotted using a linear scale.

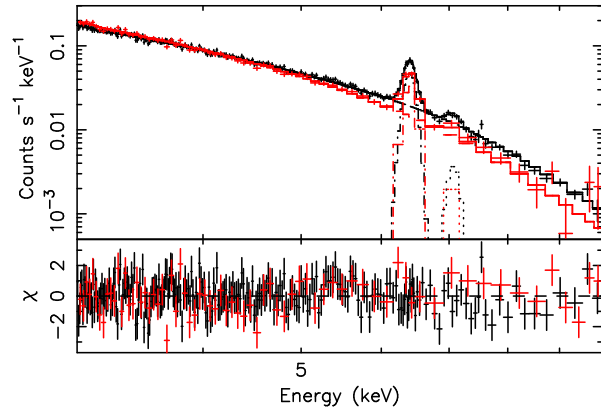


Fig. 5. Background-subtracted spectra in the hard energy band (>3 keV). Data points of XIS 0+2+3 and XIS 1 are shown with black and red crosses, respectively. Solid lines show the best-fit model of a power-law function plus two Gaussians.

version 2006-05-24 assuming uniform emission from the spectral region. A power law plus two Gaussians yields an acceptable fit ($\chi^2/\text{degree of freedom (dof)} = 270.7/291$) with the best-fit parameters given in Table 2. The best-fit model is shown in Figure 5. Note that there is a systematic error of about 15 eV in the centroid energy of the lines. The 7.1 keV line is detected clearly for the first time. Rho et al. (2002) fitted the hard continuum component of the Chandra spectrum with a SRCUT model (Reynolds & Keohane 1999) with a radio index $\alpha = 0.6$ and a cut-off frequency $\nu_c \sim 8 \times 10^{16}$ Hz. This model has an averaged

slope of a photon index 3.0 in the 3.0–10 keV band, and the Suzaku spectrum is almost consistent with this value.

Although the model reproduces the overall spectrum quite well, a residual feature is apparent at ~ 5.4 keV in Fig. 5. Addition of a Gaussian with a fixed σ (40 eV) improves the fit, with $\chi^2/\text{dof} = 258.5/289$. The best-fit centroid energy and the flux of the Gaussian are 5.38 (5.32–5.43) keV and $2.7 (1.5\text{--}3.9) \times 10^{-6}$ photons $\text{cm}^{-2} \text{s}^{-1}$, respectively. The centroid energy is consistent with the $K\alpha$ line energy of low-ionization chromium (5.41 keV). We find no indication for the presence of the $K\alpha$ line of low-ionization nickel (at 7.47 keV), obtaining a 90% upper limit for the flux $F_{Ni} < 3.3 \times 10^{-6}$ photons $\text{cm}^{-2} \text{s}^{-1}$.

In order to distinguish between the instrumental and intrinsic width of the Fe-K lines, we compared them with

Table 2. Best-fit parameters of the hard X-ray emission with a power-law function plus two Gaussians.

Parameters	Values
Power-law	
Γ	3.17 (3.14–3.19)
norm ^a	3.5 (3.3–3.6)
6.4 keV-line	
Center (keV)	6.404 (6.400–6.407)
σ^b (eV)	61 (56–66)
Flux ^c	5.1 (4.9–5.3)
7.1 keV-line	
Center (keV)	7.08 (7.04–7.11)
σ^b (eV)	69 (35–101)
Flux ^c	0.53 (0.40–0.69)
N_H (cm ⁻²) . . .	5×10^{21} (fixed)
χ^2/dof	270.7/291

Notes. Error regions correspond to 90% confidence levels.

^aNormalization at 1 keV ($\times 10^{-2}$ photons keV⁻¹ cm⁻² s⁻¹).

^bThis value includes detector energy resolution (see text).

^cTotal flux ($\times 10^{-5}$ photons cm⁻² s⁻¹) in the line.

the values derived from an identical analysis for the Sgr C observation (Table 1) which was performed 8 days after the RCW 86 observation. The 1σ width of 6.4 keV in the Sgr C observation is 39 (34–44) eV. Since the 6.4 keV line from Sgr C, a molecular cloud, is expected to have negligible intrinsic width compared with the XIS energy resolution, this width is thought to represent the instrumental energy resolution. Therefore, the difference of the 6.4 keV line widths between these two observations yields the intrinsic width of the 6.4 keV line from RCW 86, which is calculated to be 47 (34–59) eV (99% confidence). A similar analysis for the 7.1 keV line yields a width of 57 (<115) eV; a narrow 7.1 keV line cannot be excluded.

5. Discussion

The morphology of the 6.4 keV line emission has been revealed for the first time by the Suzaku observation, and shows that the line and the continuum emissions have different origins, even though both arise from the inner part of the shell and are likely to come from ejecta.

We first discuss the low-ionization plasma scenario for the 6.4 keV line. From the absence of L-shell lines Borkowski et al. (2001a) have pointed out that M-shell electrons have to be still bound. The Fe K_β line, which was detected for the first time with Suzaku/XIS, provides a clearer constraint on the ionization state of iron. The intensity ratio between Fe K_α and K_β lines, which is calculated to be 0.10 (0.074–0.14) (90% error region), is consistent with neutral iron, and shows that even if iron is ionized the mean charge is at most +12 (e.g., Palmeri et al. 2003; Mendoza et al. 2004). The Fe K_α and K_β centroid energies are also consistent with a low ionization state (e.g., Palmeri et al. 2003; Mendoza et al. 2004).

According to Porquet et al. (2001), in plasmas of almost all temperatures found in SNRs (5×10^6 – 8×10^7 K), iron is ionized to a mean charge of +9–10 when the ionization parameter $n_e t$ is 10^9 cm⁻³ s. If we interpolate the curves for $n_e t = 10^9$ and 10^{10} cm⁻³ s, the mean charge of +12 corresponds to $n_e t \sim 3 \times 10^9$ cm⁻³ s. Therefore, $n_e t$ has to be $\sim 3 \times 10^9$ cm⁻³ s or smaller. If we assume the plasma age is older than 1000 yr, the electron number density n_e in the plasma has to be smaller than 0.1 cm⁻³.

In order to produce the strong Fe K_α line by electron inner shell ionization, there have to be a lot of electrons which have higher energies than the Fe-K edge (7.1 keV). Such electrons may exist in Maxwellian or non-Maxwellian distribution. As a former case, we assume a NEI plasma (Borkowski et al. 2001b) of $kT_e = 5$ keV and $n_e t = 1 \times 10^9$ cm⁻³ s. In this case, the emission measure $\int n_e n_{Fe} dV$ has to be 1.4×10^{53} cm⁻³. The elliptical extraction region of 12'5 \times 9'2 corresponds to 11×8 pc² at 3 kpc. Assuming a uniform density of a prolate spheroid with $11 \times 11 \times 8$ pc³ axes, we arrive at $n_e n_{Fe} = 9.1 \times 10^{-6} d_{3kpc}^{-1}$ cm⁻⁶. If we apply the upper limit of the electron density, then the iron density n_{Fe} has to be larger than $9.1 \times 10^{-5} d_{3kpc}^{-1}$ cm⁻³. This density corresponds to an iron mass of $\sim 1.3 \times 10^{32} d_{3kpc}^2$ g or $\sim 0.07 M_\odot$, which is feasible to have arisen as ejecta. The largest equivalent width of the Fe K_α line found in Fig.2 is 1.3 keV. For an NEI plasma with $kT_e = 5$ keV and $n_e t = 1 \times 10^9$ cm⁻³ s, this equivalent width corresponds to an iron abundance of ~ 2.4 solar. Since most of the detected continuum emission arises in a different region from the Fe K_α line, this value represents a lower limit for the Fe abundance. Therefore, iron is likely to originate from ejecta.

If only collisional interaction is taking place between electrons and ions, the equipartition between them will not be reached at $n_e t \sim 10^9$ cm⁻³ s (Itoh 1984). Since we can assume $T_i \gg T_e$, by substituting $Z = A = 1$ (corresponding to hydrogen or proton) to equation (3) of Laming (2001), the temperature of proton T_i is calculated to be

$$T_i = 14 \left(\frac{n_e t}{1 \times 10^9 \text{ cm}^{-3}} \right)^{-1} \left(\frac{kT_e}{5 \text{ keV}} \right)^{\frac{5}{2}} \text{ MeV}. \quad (1)$$

This proton temperature corresponds to a shock speed of 8×10^4 km s⁻¹, which is too high for a shock in an SNR. Therefore, protons should have a significantly lower temperature and electrons have to be heated by some process other than Coulomb collisions. The most plausible mechanism is collisionless heating in SNR shocks (see Laming 2000). If electrons are heated by collisionless mechanism, the distribution of electrons can be non-Maxwellian or non-thermal function. However, since no continuum X-ray emission associated with the 6.4 keV line is detected, we can give no observational constraint on the distribution function of electrons.

The Suzaku observation shows that hard X-ray continuum interior to the shell is not related to the 6.4 keV line, and therefore likely to be synchrotron emission. In

order to meet the conditions for synchrotron X-ray emission under the standard diffusive shock acceleration model (e.g., Drury 1983), the shock velocity has to be larger than $\sim 2000 \text{ km s}^{-1}$ independent of the magnetic field strength (Aharonian & Atoyan 1999). This value is discrepant with the blast-wave velocity of $\sim 400\text{--}900 \text{ km s}^{-1}$ determined from observations of Balmer-dominated shocks (Ghavamian et al. 2001). It is plausible that shocks in the inner part of the shell may have higher velocity than the forward shock. The intrinsic width of $\sim 47 \text{ eV}$ found for the 6.4 keV line may be evidence of this high velocity. The forward shock might have decelerated by colliding with a cavity wall, while the inner shock relatively undecelerated within the cavity. Alternatively, a reflected shock after the collision between the forward shock and the interstellar medium structure to the southwest may be propagating back into the cavity. A cavity wall interaction of RCW 86 has also been suggested to explain the overall morphology (Vink et al. 1997) and the synchrotron X-ray emission in the north-east region (Vink et al. 2006). Finally, in this complex region, it is possible that projection effects cause an apparent superposition of an interacting shock and a much faster, relatively unimpeded one.

Finally, an observation with higher energy resolution of the SW region is highly encouraged. A stricter constraint on the iron ionization state can be obtained by measuring the difference between the centroid energies of the 6.4 and 7.1 keV lines at several eV resolution (e.g., Palmeri et al. 2003; Mendoza et al. 2004). The intrinsic width of the 6.4 keV line and existence of Cr-K line can also be verified clearly.

6. Summary

With the large effective area and low background of XIS in the hard X-ray band, we obtained following observational results regarding the hard X-ray continuum and Fe-line features from the SW region of RCW 86.

1. The spatial distribution of the 6.4 keV line is revealed for the first time. The line emission has a distinct morphology from that of the hard X-ray continuum emission.
2. The Fe $K\beta$ line is detected for the first time.
3. The Fe $K\alpha$ line is intrinsically broadened with a width of about 50 eV.

These results are all consistent with a model in which the 6.4 keV line is emitted from a low-ionization plasma of Fe-rich ejecta. The different morphology between the hard continuum 6.4 keV line emission supports the interpretation of the hard continuum as synchrotron emission.

We thank all the *Suzaku* members. M.U., R.S., H.N., and H.Y. are supported by JSPS Research Fellowship for Young Scientists. JPH acknowledges support by NASA grant No. NNG05GP87G.

References

Aharonian, F. A., & Atoyan, A. M. 1999, *A&A*, 351, 330

- Bamba, A., Koyama, K., & Tomida, H. 2000, *PASJ*, 52, 1157
 Bocchino, F., Vink, J., Favata, F., Maggio, A., & Sciortino, S. 2000, *A&A*, 360, 671
 Borkowski, K. J., Rho, J., Reynolds, S. P., & Dyer, K. K. 2001a, *ApJ*, 550, 334
 Borkowski, K. J., Lyerly, W. J., & Reynolds, S. P. 2001b, *ApJ*, 548, 820
 Cappellari, M., & Copin, Y. 2003, *MNRAS*, 342, 345
 Diehl, S., & Statler, T. S. 2006, *MNRAS*, 368, 497
 Drury, L. O. 1983, *Reports of Progress in Physics*, 46, 973
 Ghavamian, P., Raymond, J., Smith, R. C., & Hartigan, P. 2001, *ApJ*, 547, 995
 Hwang, U., Decourchelle, A., Holt, S. S., & Petre, R. 2002, *ApJ*, 581, 1101
 Hughes, J. P., Rakowski, C. E., Burrows, D. N., & Slane, P. O. 2000, *ApJL*, 528, L109
 Itoh, H. 1984, *ApJ*, 285, 601
 Koyama, K., Petre, R., Gotthelf, E. V., Hwang, U., Matsuura, M., Ozaki, M., & Holt, S. S. 1995, *Nature*, 378, 255
 Koyama, K., et al. 2006, *PASJ*, this volume
 Laming, J. M. 2000, *ApJS*, 127, 409
 Laming, J. M. 2001, *ApJ*, 546, 1149
 Mendoza, C., Kallman, T. R., Bautista, M. A., & Palmeri, P. 2004, *A&A*, 414, 377
 Mitsuda, K., et al. 2006, *PASJ*, this volume
 Palmeri, P., Mendoza, C., Kallman, T. R., Bautista, M. A., & Meléndez, M. 2003, *A&A*, 410, 359
 Petre, R., Allen, G. E., & Hwang, U., 1999, *Astron. Nachr.*, 320, 199
 Porquet, D., Arnaud, M., & Decourchelle, A. 2001, *A&A*, 373, 1110
 Reynolds, S. P., & Keohane, J. W. 1999, *ApJ*, 525, 368
 Rho, J., Dyer, K. K., Borkowski, K. J., & Reynolds, S. P. 2002, *ApJ*, 581, 1116
 Rosado, M., Ambrocio-Cruz, P., Le Coarer, E., & Marcelin, M. 1996, *A&A*, 315, 243
 Serlemitsos, P., et al. 2006, *PASJ*, this volume
 Slane, P., Hughes, J. P., Edgar, R. J., Plucinsky, P. P., Miyata, E., Tsunemi, H., & Aschenbach, B. 2001, *ApJ*, 548, 814
 Takahashi, T., et al. 2006, *PASJ*, this volume
 Vink, J., Kaastra, J. S., & Bleeker, J. A. M. 1997, *A&A*, 328, 628
 Vink, J., Bleeker, J., van der Heyden, K., Bykov, A., Bamba, A., & Yamazaki, R. 2006, *ApJL*, 648, L33
 Whiteoak, J. B. Z., & Green, A. J. 1996, *A&AS*, 118, 329